Dissipative switching waves and solitons in the systems with spontaneously broken symmetry

D. Dolinina* and A. Yulin†
Faculty of Physics, ITMO University, Saint-Petersburg 197101, Russia

(Received 16 February 2021; accepted 15 April 2021; published 7 May 2021)

The paper addresses the bistability caused by spontaneous symmetry breaking bifurcation in a one-dimensional periodically corrugated nonlinear waveguide pumped by coherent light at normal incidence. The formation and the stability of the switching waves connecting the states of different symmetries are studied numerically. It is shown that the switching waves can form stable resting and moving bound states (dissipative solitons). The protocols of the creation of the discussed nonlinear localized waves are suggested and verified by numerical simulations.

DOI: 10.1103/PhysRevE.103.052207

I. INTRODUCTION

It has been known that in bistable nonlinear systems, two different spatially uniform states can be connected by a switching wave preserving its shape. These structures have first been reported in [1] and then found in many optical systems [2–6]. The integrity of the domain wall is supported by the exact balance of different linear and nonlinear effects such as diffraction, the dependency of the effective refractive index on the light intensity, linear and nonlinear losses, the external pump, etc. In these respects, the domain walls are similar to nonlinear localized waves called solitons. It is important to note that the domain walls connecting different spatially uniform states can be at rest (this is so-called Maxwell point), but the general case is when domain walls are moving. The motion of a domain wall results in the expansion of one of the uniform states and to the shrinking of another, and this is why these localized structures are called switching waves. Let us remark that these switching waves are also often referred to as domain walls because they separate different states. In the present paper, we use both terms.

If two or more domain walls have formed in a system, then they can interact with each other provided that the distance between the domain walls is comparable to their characteristic size. In some cases, this interaction can result in the formation of bound states of the switching waves. These bound states can also be seen as dissipative solitons [7–14]. The dissipative solitons play an important role in optics; for example, they are used for the generation of femtosecond pulses in fiber lasers [15,16]. This explains why dissipative optical solitons have been actively studied for many years.

In the present paper, we consider dissipative localized waves in optical systems where there may exist modes of different symmetries that have very different losses. These systems are related to the so-called optical bound states in continuum (BIC) that are actively studied now because this phenomenon opens a way to achieve solitary high-Q resonances. BIC systems have already been used for second and third harmonic generation [17,18] and in laser design [19].

The characteristic feature of BIC states is that they cannot be directly excited by the external coherent light, and therefore they are often referred to as dark states (DS). The states coupled to free propagating waves have higher losses, but can be directly excited; these states are called bright states (BS). It is obvious that in the presence of the finite intrinsic losses, no stationary states can have a structure of pure DS. However, the BS can be unstable against the linear excitations having a structure of DS. This instability breaks the symmetry of the solution, leading to the formation of hybrid states (HS) that can be seen as a combination of BS and DS. It is important to note that the dominating component of HS can be of the DS kind and, thus, HS can experience very low effective losses and so they can exist at lower levels of pump intensities. This can facilitate the experimental observation of optical bistability and other nonlinear effects.

For our purposes, we do not need a true BIC when, for some modes, the radiative losses vanish completely, but a quasi-BIC when the radiative losses of some modes are significantly depressed by destructive interference. In the general case of a quasi-BIC, the quasi-DS can weakly interact with nonguided waves, but within the model used in this paper, these losses are accounted for as effective intrinsic losses of DS. Recently it was shown that bright dissipative solitons can nestle on the HS in such systems; see [20]. The aim of the present paper is to study the domain walls connecting different spatially uniform states. It will be shown that the domain walls connecting HS and BS exist, can be dynamically stable, and can form stable bound states.

It is well known that the symmetric systems can have asymmetric soliton solutions and that the symmetry breaking sets the dissipative solitons in motion [21–31]. Let us remark that symmetry breaking bifurcation is also known for connecting two physically equivalent spatially uniform states. In this case, the symmetry breaking transforms a resting Ising-type domain wall into a moving domain wall of the Bloch kind [32–35]. In addition, recently it was demonstrated that the nonlocal

*d.dolinina@metalab.ifmo.ru
†a.v.yulin@corp.ifmo.ru

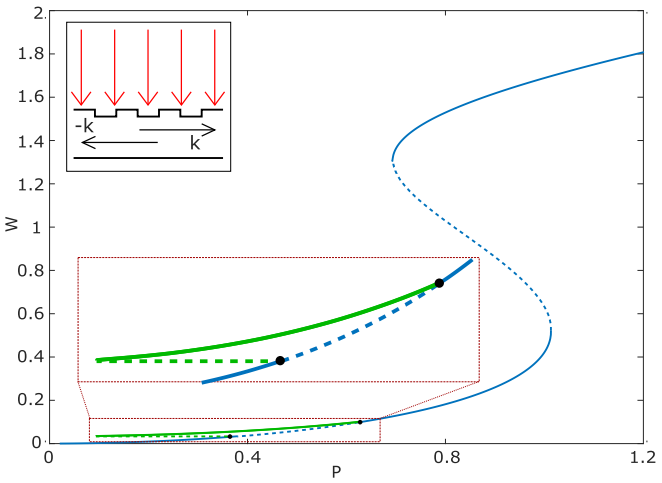

FIG. 1. Bifurcation diagram of the bright (blue line) and hybrid (green line) states, where $W = |U_b|^2 + |U_d|^2 = |U_+|^2 + |U_-|^2$ is the intensity of states; dynamically unstable solutions are shown by the dashed line. Parameters are $\delta = 0.05$, $\alpha = -1$, $\sigma = 1$, $\gamma = 0.001$, and $\Gamma = 0.299$. The inset shows a schematic view of the considered system.

Raman response sets the localized structures in motion [36–38]. In our paper, we discuss both the resting and moving dissipative solitons, but in our case, the motion of the solitons is caused by the broken symmetry of the solitons' pedestals and the type of the soliton pedestal defines the direction of the soliton motion.

The article is organized as follows. In Sec. II, we briefly discuss the physical system and formulate the mathematical model describing it. In this section, we also summarize important facts regarding the structure and the stability of the spatially uniform states. The formation and the stability of the switching waves connecting spatially uniform states of different symmetries are studied in Sec. III. Section IV is devoted to the bound states of the switching waves, i.e., to dissipative solitons. In this section, we also suggest protocols that allow one to observe the dissipative solitons in the experiments. Finally, in the conclusion, we list the main results of the paper.

II. THE PHYSICAL SYSTEM AND ITS MATHEMATICAL MODEL

As a system possessing quasi-BIC states, we consider externally pumped one-dimensional waveguides with periodical grating and Kerr nonlinearity, as schematically shown in the inset of Fig. 1 (taken from Fig. 1(a) of [20]). The resonant scattering on the periodical grating results in the appearance of a gap in the dispersion characteristics and to a dramatic decrease of the eigenwaves group velocity, which becomes equal to zero at the exact resonance. It is worth noting that the upper and lower modes can experience very different radiative losses. A simple explanation of this is that each mode can be seen as a composition of two counterpropagating waves. Each of the counterpropagating waves can leak from the waveguide, but the total radiative losses are defined by the interference of the contributions from each of the counterpropagating waves. In the case of destructive interference, the contributions from the counterpropagating waves cancel each other and, thus, the radiative losses get suppressed. The constructive interference enhances the radiative losses.

The dynamics of the system is described as in [39] by a two counterpropagating waves approach and can be expressed mathematically by the following system of equations:

$$(\partial_t \pm \partial_x)U_\pm = (i\delta - \gamma)U_\pm + i\alpha(|U_\pm|^2 + 2|U_\mp|^2)U_\pm + (i\sigma - \Gamma)(U_\pm + U_\mp) + P, \quad (1)$$

where U_+ and U_- are the slow varying complex amplitudes of the two counterpropagating waves, δ is the detuning of the frequency of the pump from the center of the gap of the dispersion characteristics, γ are the losses of different nature that cannot be compensated for by the U_+ and U_- waves interference, $\alpha = \pm 1$ is the Kerr-nonlinearity coefficient, σ is the conservative part of the coupling coefficient defining the rate of the mutual rescattering of the counterpropagating waves, and Γ is the dissipative coupling accounting for the fact that the radiative losses depend on the interference of the waves.

It is convenient to reformulate the problem in terms of the complex amplitude of bright modes, $U_b = \frac{U_+ + U_-}{\sqrt{2}}$, and dark modes, $U_d = \frac{U_+ - U_-}{\sqrt{2}}$. With these variables, Eq. (1) reads

$$\left(\partial_t - i\delta - i\frac{3}{2}K + \gamma + 2\Gamma - 2i\sigma\right)U_b + (\partial_x + iM)U_d = 2P, \quad (2)$$

$$\left(\partial_t - i\delta - i\frac{3}{2}K + \gamma\right)U_d + (\partial_x + iM)U_b = 0, \quad (3)$$

where $K = \alpha(|U_b|^2 + |U_d|^2)$ and $M = \alpha Re(U_b U_d^*)$. From (2) and (3), it is seen that linear eigenmodes in the form $e^{-i\omega t + ikx}$ with $k = 0$ have the structure ($U_b \neq 0$, $U_d = 0$) and ($U_b = 0$, $U_d \neq 0$). The second mode has only intrinsic losses $\gamma_d = \gamma$ and, thus, the losses are lower than the losses of the first mode, $\gamma_b = \gamma + 2\Gamma$. It is also obvious from Eq. (3) that the second mode cannot be excited by the driving force accounting for the action of the pumping wave at normal incidence. Thus, this mode is the dark one. The first mode can be excited by the pump and so it is a bright mode. In the nonlinear regime, there may exist the states such that both their components are nonzero, $U_b \neq 0$, $U_d \neq 0$ [20,39]. These modes are the hybrid nonlinear modes.

As it is shown in [39], the spatially uniform hybrid states are always unstable for $\alpha = 1$ and, therefore, we consider only the case $\alpha = -1$. To facilitate the discussion of the nonlinear localized waves and, in particular, switching waves, we briefly reproduce the results on the formation and stability of the spatially uniform states reported in [20]. Stationary nonlinear states can be classified as bright states (BS) with $U_b \neq 0, U_d = 0$ and as hybrid states (HS) with $U_{b,d} \neq 0$. The bifurcation diagram of the BS is shown in Fig. 1 by the blue curve. The HS bifurcating from the BS are shown by the green curve. The spectral linear stability analysis as well as direct numerical simulations show that the HS belonging to the upper branch of the bifurcation curve are stable and, thus, are of interest from a physical point of view.

Here we acknowledge an important fact that the hybrid states are produced by the spontaneous symmetry breaking and, therefore, they consist of two counterpropagating waves

of different amplitudes, $|U_+| \neq |U_-|$, and so these are the states with energy flow $F_{HS} = |U_+|^2 - |U_-|^2$ directed either from the left to the right or from the right to the left. The symmetry of the equations $x \to -x$, $U_\pm \to U_\mp$ insures that if $U_+ = a$, $U_- = b$ is a spatially uniform solution, then $U_+ = b$, $U_- = a$ is also a spatially uniform solution. Thus, the spatially uniform HS are double degenerate and have the energy flux of the same absolute value but of different signs.

III. DOMAIN WALLS CONNECTING THE HYBRID AND BRIGHT STATES

In this section, we consider the stationary domain walls connecting different spatially uniform HS to spatially uniform BS. To find stationary solutions, we set to zero the temporal derivatives and thus reduce the system (1) to a system of ordinary differential equations. Then, substituting the derivatives by their discrete analogues, we approximate the ordinary differential equations by a system of nonlinear algebraic equations. The algebraic system is solved numerically by the iteration method. The linear stability of the stationary solutions is examined by finding the eigenmodes of the weak perturbations of the stationary solution. The dynamics of these excitations is described by linear equations with coefficients being functions of the spatial coordinate. To find the eigenvalues and eigenmodes of the perturbation, we substitute the spatial derivatives by their discrete analogues and then solve the corresponding spectral problem numerically. The existence of the modes growing in time means that the background state is dynamically unstable. The growth rate is defined by the real part of the eigenvalue of the mode and thus if the spectrum of the perturbation contains one or more eigenvalues with positive real part, then the examined solution is unstable. To check the results of the spectral stability analysis and to study the nonlinear stage of the instability, we performed direct numerical simulations of (1) using the split-step Fourier method; see [40]. This method is proven to be highly efficient and is widely used for modeling of different nonlinear optical systems.

Let us start with introducing the notation of the domain walls. In the present paper, we focus on the domain walls connecting the stable hybrid states to the bright states belonging to the lower branch of the bifurcation characteristics. Then it is possible to mark the domain walls by the kinds of spatially uniform states connected by the domain walls. For example, a domain wall BH is a connection of the bright state on the left to the hybrid state on the right. Then, HB is a domain wall where the bright and the hybrid states are swept (HS is on the left side of the domain wall and BS is on the right). It is important to note that the characteristic size of the domain walls should be much larger than the grating period; otherwise the slowly varying amplitude approximation is not applicable and new effects appear [41].

As mentioned above, the hybrid states have nonzero energy flux and so we need to distinguish the hybrid states where energy flows from the left to the right from the hybrid states with opposite direction of the energy flow. We denote the former ones as H_+ and the latter as H_-. The bright states have zero energy flux and will be marked as B without indices. Let us emphasize that from a physical point of view, it is obvious that the domain walls H_+B and H_-B are different; in the first case, the energy flow in the HS is directed towards the domain wall, and in the second case, it is directed away from the domain wall.

The linear analysis of the stationary perturbations on the $H_\pm S$ and BS background has revealed that the small excitations can exponentially decay with or without oscillations to the backgrounds. Therefore, one can expect that the states can be connected by domain walls with exponential tails. As mentioned before, the domain walls move with some velocity which depends on the parameters of the system. The assumption that the domain wall is moving without changing its shape allows one to look for this solution in a moving reference frame where the domain wall field distribution depends only on the coordinate $\xi = x - vt$ and so is described by ordinary differential equations. The equations have to be solved with the boundary conditions corresponding to the prescribed spatially uniform states on the left and on the right. From the mathematical point of view, a domain wall is a heteroclinic phase trajectory connecting two different equilibrium points in the phase space of the differential equation written in the moving reference frame. These trajectories do not exist for an arbitrary velocity, but for some values of v the heteroclinic trajectories can be found. We solved the corresponding boundary value problem numerically and found the domain walls connecting the upper hybrid state to the lower bright state; a typical bifurcation diagram v vs P of the domain walls is shown in Fig. 2(b).

Let us first discuss the domain walls H_+B connecting the state H_+ on the left and B on the right. The dependency of the velocity of the domain walls on the pump is shown for typical parameters in Fig. 2(b) by the black line. One can see that there is a special value of the pump called a Maxwell point (due to analogy with thermodynamics) at which the velocity of the domain wall is zero. The existence of resting domain walls is known in many physical systems, including optical ones [1,3,4,42]. The existence of the Maxwell point in our system is important for the formation of the dissipative solitons (bound states of domain walls) that are considered in the next section in detail.

The range of the existence of H_+B almost coincides with the range of the existence of the stable HS [the upper branch of the HS bifurcation curve shown in Fig. 2(a)]. The domain wall is wide for the low pump intensities; numerical simulations indicate that the domain wall width goes to infinity at the left border of the existence domain. Typical distributions of the domain wall fields are shown in Figs. 3(a)–3(c) for different intensities of the pump.

Let us remark here that it is also possible to find other family of H_+B domain walls; see Fig. 2(b) where the corresponding branch of the bifurcation diagram is shown by a blue dashed line. These domain walls have a more complex structure, but we did not manage to find stable domain walls of such a kind.

Another important remark is that because of the symmetry $x \to -x$, $U_\pm \to U_\mp$ of Eq. (1), the domain walls BH_- can be obtained from the domain walls H_+B by the inversion of the direction of the x axis and the swap of the fields $U_\pm$; compare Figs. 3(a)–3(c) and Figs. 3(d)–3(f), showing the field distributions in H_+B and BH_- domain walls for the same

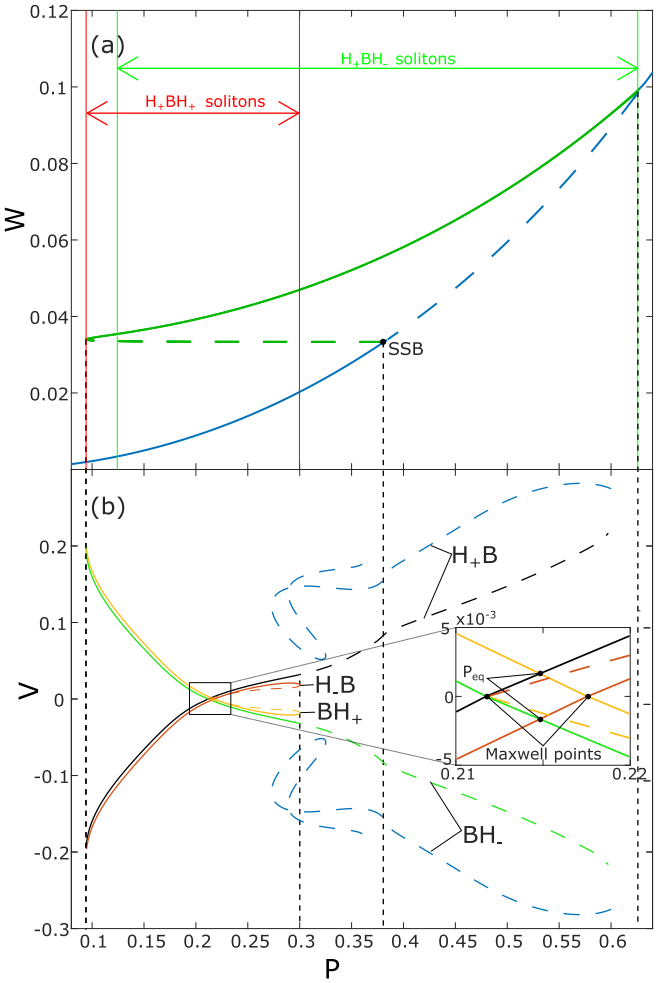

FIG. 2. (a) The part of the bifurcation diagram showing the dependencies of the intensities of the hybrid and bright (belonging to the lower branch) spatially uniform states on the pump amplitudes. Two vertical dashed lines mark the range of the existence of the stable hybrid states. The green lines and arrows show the range of the existence of resting H_+BH_- and H_-BH_+ solitons. The range of existence of moving H_+BH_+ and H_-BH_- solitons is shown by the red lines and arrows. The point where the bright states become unstable is marked as SSB. (b) Velocity dependencies of the domain walls on the pump. The bifurcation curves of the different domain walls are shown by different colors. The solid lines correspond to the stable domain walls and the dashed lines to the unstable domain walls. The inset shows the enlarged region near the Maxwell points of H_+B and BH_+ domain walls. The points where the domain walls H_+B and BH_+ (or H_-B and BH_-) have equal velocities are marked as P_{eq}.

pump intensities. For a fixed pump, the velocities of H_+B and BH_- domain walls are of the same absolute value but of different sign; see the bifurcation diagrams of the domain walls presented in Fig. 2(b).

Now let us discuss an important issue of the dynamical stability of the domain walls. It is obvious that if one of the backgrounds of the domain wall is unstable, then the whole state is unstable and, thus, the domain walls existing to the right from the point of the SSB (spontaneous symmetry breaking bifurcation destabilizing the lower bright state) are always unstable. However, the linear stability analysis shows that the

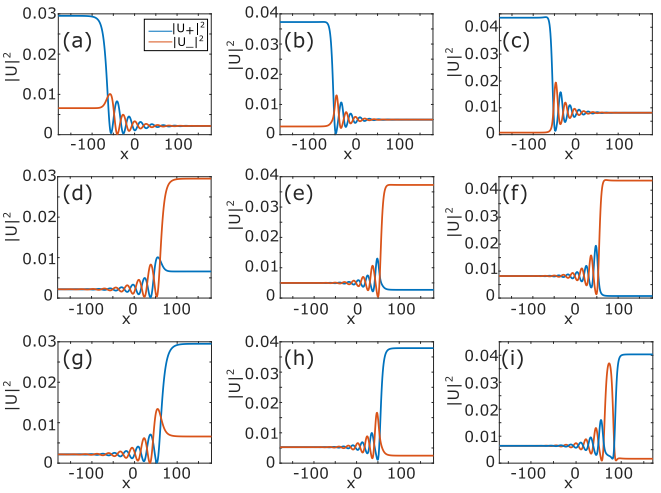

FIG. 3. Field distributions of the domain walls. (a) H_+B at $P = 0.14$, (b) H_+B at Maxwell point, (c) H_+B at $P = 0.27$, (d) BH_- at $P = 0.14$, (e) BH_- at Maxwell point, (f) BH_- at $P = 0.27$, (g) BH_+ at $P = 0.14$, (h) BH_+ at Maxwell point, and (i) BH_+ at $P = 0.24$ of the unstable branch.

domain wall loses its stability at the pump values lower then that of SSB. The simulations of Eq. (1) confirmed that for relatively low pump intensity, the backgrounds remain stable but the domain wall gets destroyed; see Fig. 4 showing the development of the instability.

The instability results in the development of an oscillating pattern separating the HS and BS. At longer times, the hybrid state expands, but stable dark solitons stay incorporated in the HS. The interaction between the dark solitons leads to their collision and annihilation; this process is seen well in Fig. 4. However, the interaction between the solitons decreases exponentially with the distance. Therefore, the HS with incorporated solitons can be seen as a metastable state. We remark here that the oscillation pattern can be an indication of the existence of a periodic nonlinear state, but this problem requires a separate consideration and is beyond the scope of the present paper.

Another kind of domain walls considered in this paper is H_-B or BH_+ which are related to each other by the inversion of the x axis and the swap of the fields. Their bifurcation diagrams are shown in Fig. 2(b) by the red and yellow curves. The typical field distributions in the BH_+ for different pump intensities are shown in Figs. 3(g)–3(i). At low pumps, the domain walls are wide, with the width going to infinity at the left end of the bifurcation diagram.

At some pump, the domain wall experiences a fold bifurcation and becomes unstable. The domain wall belonging to the lower unstable branch of the bifurcation diagram can be seen as an equilibrium combination of a BH_+ domain wall and a dark soliton. This becomes obvious at the left end of the bifurcation curve, where the distance between the domain wall and the soliton goes to infinity.

The structure of these domain walls suggests the possible mechanism of their instability. If the distance between the soliton and the domain wall becomes smaller, then the soliton gets attracted and collides with the domain wall. Alternatively,

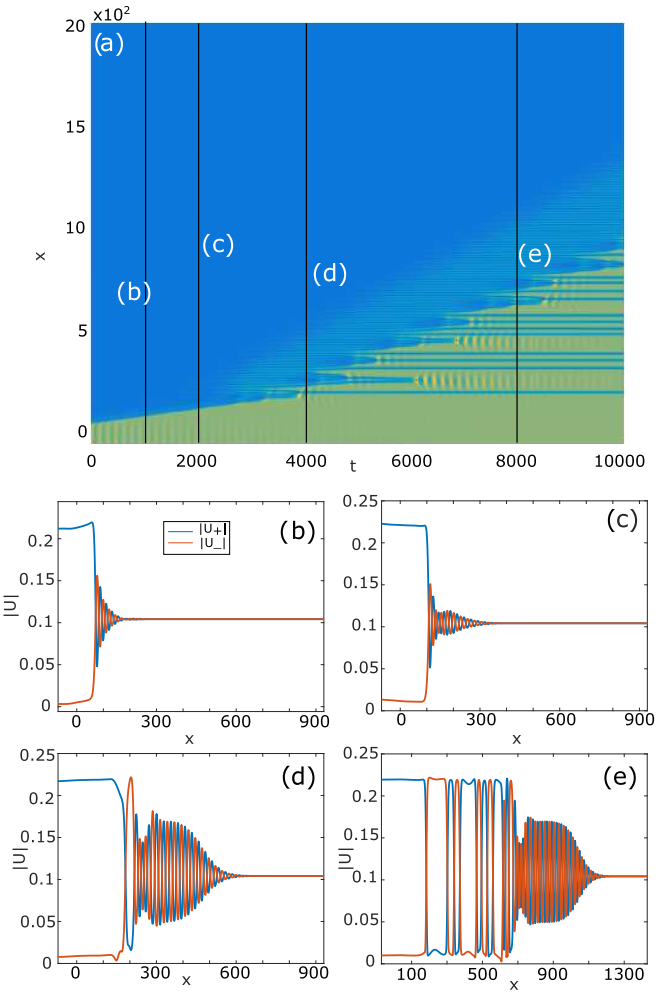

FIG. 4. (a) The evolution of the unstable H_+B wall at $P = 0.31$ obtained by numerical simulations of Eq. (1). The colors shows the total intensity of the state $|U_+|^2 + |U_-|^2$: the blue color corresponds to the lowest intensity and the yellow color corresponds to the highest intensity. (b)–(e) The distribution of the fields at different times.

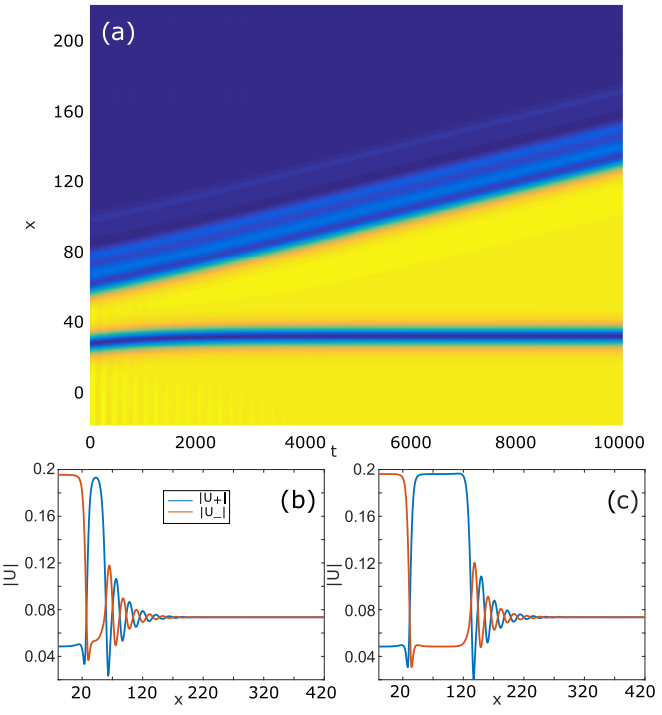

FIG. 5. (a) The evolution of the unstable H_-B domain wall at $P = 0.22$ obtained by numerical simulations of Eq. (1). The colors show the total intensity of the state, $|U_+|^2 + |U_-|^2$: the blue color corresponds to the lowest intensity and the yellow color corresponds to the higher intensity. (b) Numerically found unstable domain wall taken as the initial conditions for the numerical simulations shown in (a). The domain wall can be seen as an unstable bound state of the H_+B wall and a dark soliton (H_-BH_+ soliton) used as an initial condition in the numerical simulation. (c) Field intensity distributions at $t = 10\,000$.

if the distance between the soliton and the domain wall increases, then they depart from each other. Numerical simulations fully confirmed this guess. The development of the H_-B domain wall instability is illustrated in Fig. 5. It is clearly seen that the development of the instability results in the formation of a resting dark soliton and the domain wall moving away from the soliton.

Considering the nature of the instability, it can be concluded that the instability growth rate becomes small at low pumps where the domain wall and the dark soliton are well separated and, thus, interact very weakly. At the fold bifurcation, the instability growth rate also goes to zero, and thus the maximum instability growth rate is inside the region of the domain wall existence. The numerical analysis shows that the point of the maximal instability growth rate is shifted towards the fold bifurcation point.

In this section, it is shown that in the considered system, there are several kinds of domain walls and that some of the domain walls are stable. It was also shown that the instability can result in the formation of dark solitons that can be seen as stable bound states of two domain walls. This calls for systematic studies of the dissipative solitons that occur in the system. This is the subject of the next section.

IV. DARK SOLITONS

In this section, we discuss different dissipative solitons that can be interpreted as bound states of the domain walls connecting the lower bright and the hybrid spatially uniform states.

We start with the solitons that are formed by the domain wall H_+B on the left and domain wall BH_- on the right. As discussed above, the hybrid states forming these domain walls are related by the operation of simultaneous inversion of the spatial coordinate and the swap of the fields $U_\pm$. Each of the hybrid states H_+ on the left and H_- on the right have the energy flow directed towards the bound state formed by the domain walls. The intensity of the field in the center of the bound state is lower than the intensity of the backgrounds, and so the bound state can be referred to as a dark dissipative soliton. We can denote the soliton as the H_+BH_- soliton, meaning that the soliton is the state consisting of the H_+B on the left and BH_- on the right. Let us note here that from the mathematical point of view, these soliton solutions are the heteroclinic trajectories connecting different stationary points

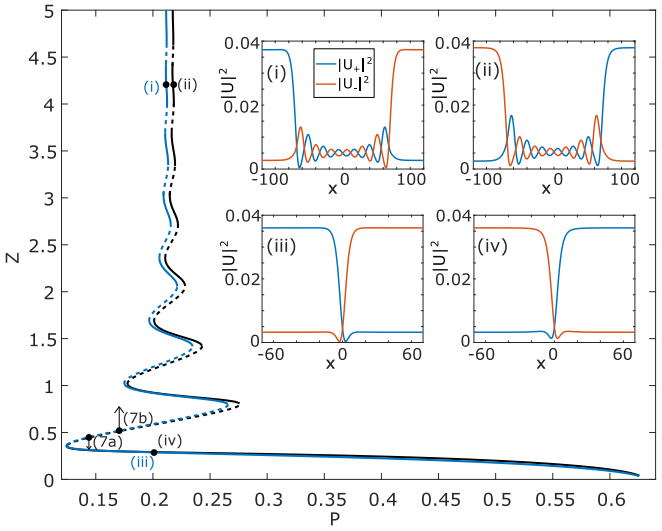

FIG. 6. Bifurcation diagrams of H_+BH_- (blue line) and H_-BH_+ (black line) solitons. The dashed lines correspond to the unstable states. It is seen that in the vicinity of the Maxwell points, the bifurcation curves form snaking patterns. Insets (i) and (ii) illustrate the field distributions of the solitons belonging to the snaking patterns of the bifurcation diagrams. These states correspond to the points (i) and (ii) of the bifurcation curves. The field distributions in the H_+BH_- and H_-BH_+ solitons at pump $P = 0.2$ are presented in insets (iii) and (iv) for H_+BH_- and H_-BH_+ solitons, respectively. The relevant points on the bifurcation curves are marked as (iii) and (iv) in the main panel.

in the phase space of the corresponding ordinary differential equation.

We calculated the bifurcation diagram of the soliton; the curve showing the dependence of the soliton width defined as $Z = \int_{-\infty}^{\infty} ||U_+|^2 + |U_-|^2 - (|U_+^0|^2 + |U_-^0|^2)|dx$ on the pump amplitude P is shown in main panel of Fig. 6 by the blue line. Strictly speaking, the Z value is not really the width, but assuming the soliton depth near the Maxwell point to be constant, Z depends only on the soliton width. The solitons exist in the whole domain of the existence of the H states. As expected, because of the symmetry of the domain walls, the discussed solitons have zero velocity.

The linear analysis of the stationary linear perturbations shows that they decay to the bright state B with oscillations and this gives a reason to expect that there may exist more than one equilibrium distance between the domain walls forming the H_+BH_- solitons. It is also important that the H_+B and BH_- domain walls have Maxwell points and that these Maxwell points are at the same pump value for both of the domain walls. To form a bound state of the resting domain walls, the interaction strength can be arbitrarily weak. Therefore, one can expect the formation of the snaking pattern of the bifurcation characteristic around the Maxwell point [10,13,43,44]. The corresponding snaking pattern is clearly seen in Fig. 6. The discussed solitons separate two different states and so the snaking is heteroclinic. Below we will show that homoclinic snaking is also possible in the considered system.

After each of the turns of the snaking pattern, the width of the dissipative soliton increases by the period of the oscillations of the domain wall tail decaying to the bright state. The distribution of the field in a soliton in the vicinity of the Maxwell point is shown in inset (i) of Fig. 6. It is seen that the soliton can indeed be considered as two remote and, thus, very weakly interacting domain walls.

The spectral analysis has revealed that in the snaking pattern, the stability of the dark solitons H_+BH_- changes at each fold bifurcation and so the stable parts of the bifurcation curve interchange with the unstable ones. The instability can be understood in terms of the effective potential created by a domain wall for its neighbor. The maxima of the potential correspond to the unstable solitons. Then one can anticipate that the development of the instability leads to the change of the distance between the domain walls. The result of the instability is the formation of a stable bound state with the width smaller or larger than the width of the initial bound state. The results of the numerical simulations illustrating the development of the instability of the H_+BH_- solitons are shown in Fig. 7(a). One can see that, indeed, the instability simply changes the width of the soliton to the width of a stable soliton. Otherwise, the instability of the bound state can result in separation of the H_+B and BH_- domain walls, as shown in Fig. 7(b).

Outside the snaking pattern, the solitons exist in the whole region of existence of the domain walls. The width of the soliton can be of the size or more narrow than the size of the domains wall; see inset (iii) of Fig. 6. The stability analysis tells us that outside the snaking pattern, solitons H_+BH_- are stable provided that the H_+ and H_- states are stable.

Another possible combination of the domain walls that can be in equilibrium and, thus, can be considered as a dissipative soliton is H_-B and BH_+ domain walls. These domain walls form the bound states where the energy on the left and on the right flows away from the bound state. The intensity distribution in these solitons is symmetric and the solitons are at rest; see insets (ii) and (iv) in Fig. 6.

In H_-BH_+ solitons, the energy flows away from the solitons and, of course, these solitons cannot be identical to H_+BH_- solitons; however, their properties are similar. In particular, the bifurcation diagram of the H_-BH_+ solitons shown in Fig. 6 by the black curve has a snaking pattern around the Maxwell point. As in the case of H_+BH_- solitons, each turn of the bifurcation curve corresponds to the increase of the soliton width by an oscillation period of the domain wall tails decaying to the BS. In the snaking pattern, the stability of the soliton changes at each turn of the bifurcation characteristics. The mechanism of the instability is also the same as in the case of H_+BH_- solitons: the solitons change their size to the size of the neighboring stable soliton. The H_-BH_+ solitons exist in the range of the existence of H_-B and BH_+ domain walls. Outside the snaking area, the solitons are stable provided that the HS on the left and on the right of the soliton are stable.

A different example of dissipative solitons is the bound states H_+BH_+ and H_-BH_-. The latter ones can be obtained from the former ones by the inversion of the x axis and the swap of the fields, $U_\pm \to U_\mp$. Therefore, they possess the same properties and so we discuss here only H_+BH_+ solitons. The peculiarity of these solitons is that because of the symmetry breaking bifurcation, the energy flows to the soliton from the left and flows out of the soliton on the right. Thus,

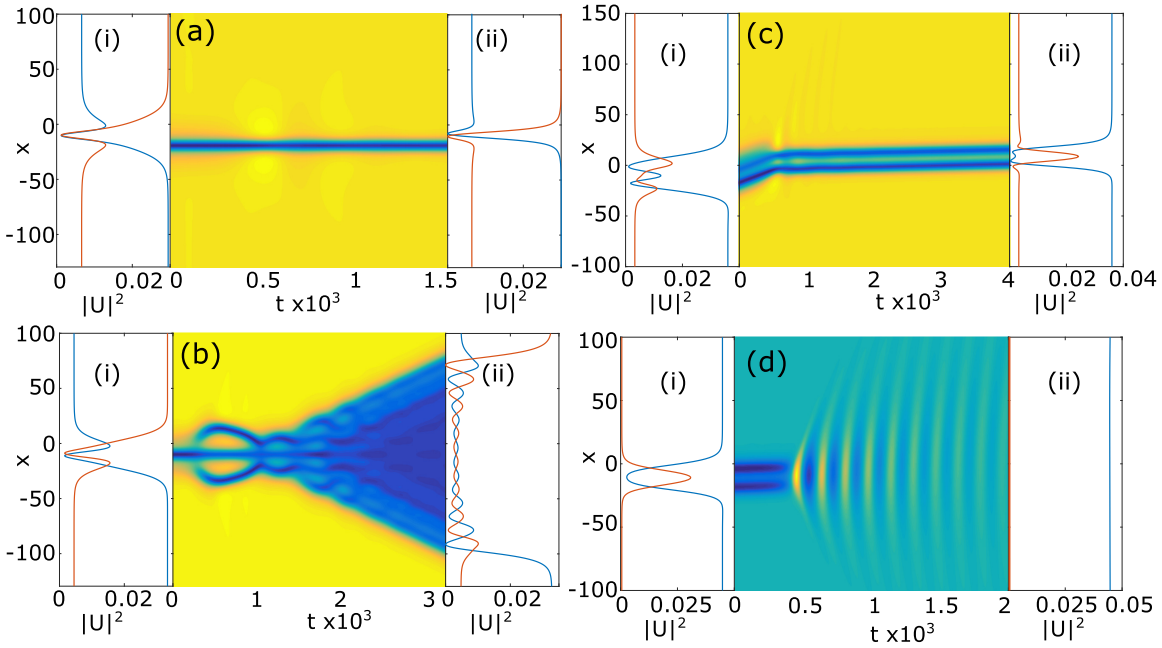

FIG. 7. (a) Development of the instability of the H_+BH_- soliton at $P = 0.14$. (i) Dynamically unstable soliton is taken as an initial condition in the numerical simulation. (ii) Resulting stable soliton with the width smaller than the initial one. (b) Development of the instability of the H_+BH_- soliton at $P = 0.17$. (i) Initial conditions in the form of an unstable soliton. (ii) The final distributions of the fields where the separation of two domain walls is clearly seen. (c) Development of the instability of the H_+BH_+ soliton at $P = 0.2$. (i) The initial condition in the form of the unstable soliton. (ii) Resulting stable soliton with the width smaller than the initial one. (d) Development of the instability of the H_+BH_+ soliton at $P = 0.28$. (i) The initial condition in the form of the unstable soliton. (ii) The final spatially uniform field distribution corresponding to the hybrid state which appears after the collapse of the soliton.

one can expect that these solitons are the moving ones. We found numerically the solitons H_+BH_+ and found out that, indeed, the solitons move with some velocity depending on the intensity of the pump; see the bifurcation diagram shown in Fig. 8(a) by the blue curve. The distribution of the field in the solitons is illustrated in Figs. 8(b) and 8(c) for different points of the bifurcation curve.

As seen in Fig. 2(b), there is a pump P_{eq} at which the domain walls H_+B and BH_+ move with the same velocity v_{eq}. One can expect that at this point, the bound state can be infinitely wide, consisting of two noninteracting domain walls. Since the stationary fields decay to the BS with oscillations, there may be more than one equilibrium distance between the domain walls forming the soliton. At the pump P_{eq}, the number of the solitons goes to infinity and, thus, the bifurcation curve swirls toward the point $P = P_{eq}$, $v = v_{eq}$ on the bifurcation diagram plotted in the $v - P$ axes. In the bifurcation diagram in the $Z - P$ axes, this results in the formation of the snaking pattern discussed above; see Fig. 8(e). Unlike the previous type of solitons, these solitons connect the same stationary states, and therefore the snaking is of the homoclinic type [45].

The problem of the stability of the solitons is of importance from the physical point of view. We studied the stability of the H_+BH_+ solitons by finding the eigenvalues governing the dynamics of the small perturbation imposed on the soliton. The analysis shows that H_+BH_+ can be dynamically stable; see Fig. 8(a) where the solid parts of the bifurcation curve correspond to stable dissipative solitons. The stability of the solitons has also been checked by direct numerical simulations of the partial differential equation, with the initial conditions taken in the form of the soliton perturbed by a weak noise. The simulations confirmed the prediction of the spectral stability analysis and shed light on possible outcomes of the instability of H_+BH_+ solitons. It turned out that the soliton can change its width to that corresponding to a stable soliton; see Fig. 7(c). Alternatively, the bound state of the domain walls forming an unstable bound state can be broken and then domain walls annihilate and the system switches to a spatially uniform H_+ state, as shown in Fig. 7(d).

Let us remark here that the bound states of the domain walls can also be bright solitons $BH_\pm B$ with the intensity having a maximum within the soliton. The bifurcation curve of these solitons is shown by the red dashed line in Fig. 8(a); a typical distribution of the fields of the soliton is illustrated in Fig. 8(d). However, we did not find stable solitons of such a kind. This makes them less interesting from the physical point of view and we do not discuss them in detail. We note that stable bright solitons exist in the system [20], but these solitons can hardly be considered as bound states of dissipative domain walls but rather as a generalization of bright nonlinear Schrödinger equation solitons for the case of driven-dissipative systems.

The discussed solitons are stable and, thus, can be observed in real experiments. We did some estimations of real pump powers required for soliton formation. For a semiconductor waveguide with the grating period 3 μm, the order of the pump power can be estimated as less than 1 kW/cm^2 [46], which is an experimentally achievable value. For recently developed highly nonlinear materials where strong light-matter

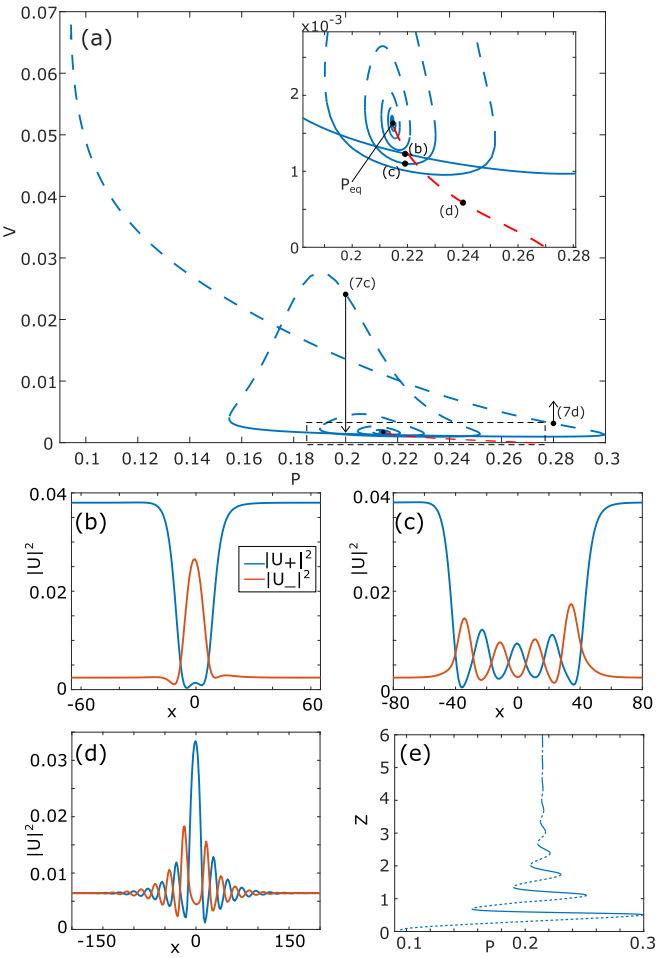

FIG. 8. (a) The velocities of H_+BH_+ (blue line) and BH_+B (red line) moving solitons as a function of the pump P. P_{eq} is the point where the domain walls H_+B and BH_+ have the same velocities; see the inset in Fig. 2(b). The fields distributions of the (b) single-hump H_+BH_+ soliton at $P = 0.22$, (c) multihump H_+BH_+ soliton at $P = 0.22$, and (d) BH_+B soliton at $P = 0.24$. The snaking of the bifurcation curve of the moving H_+BH_+ soliton around the Maxwell point is shown in (b) in the Z-P axis.

interaction takes place [47], the required pump power is anticipated to be much lower.

Another question of great importance is how these states can be created in experiments. Here we suggest the protocols that allow one to form the dissipative solitons starting from the initial condition in the form of weak noise. First we do it for the solitons H_-BH_+. To observe the solitons in the numerical simulations, we consider a straight corrugated waveguide of finite length driven by an external pump whose intensity and distribution in space can be controlled. To avoid the strong influence of the boundaries, we take the interaction strength between the counterpropagating waves to be higher in the vicinity of the edges; in the middle of the system the interaction strength is a constant. The profile of the coupling strength used in our simulations is shown by the red line in Fig. 9(a). Experimentally, this can be achieved by the increase of the modulation depth of the waveguide at its edges.

When the pump is switched on, the intensities of the field start growing and, if the pump is strong enough, then at some

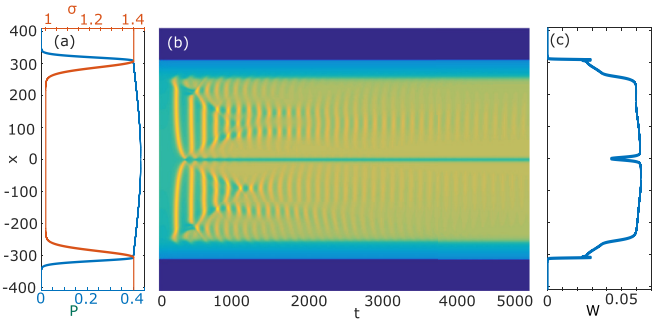

FIG. 9. The formation of the H_-BH_+ dark soliton from the weak noise taken as the initial conditions. (a) The distributions of the amplitude of the spatially nonuniform pump P shown by the blue curve. The distribution of the coupling strength coefficient σ is shown in this panel by the red curve. (b) The numerically obtained evolution of the field. (c) The final distribution of the field, where the dark soliton is clearly seen.

moment the hybrid states form. However, the boundaries introduce additional losses and, thus, the hybrid state forming at an edge has energy flow directed towards the edge. As a result of the evolution, the final state consists of two hybrid states with energy flows directed towards the edge nearest to the state. In the center of the system, the states are connected by a dark soliton; see Fig. 9(b). The profile of the field intensity of the stationary solution is shown in Fig. 9(c) and it was checked that this field distribution coincides with the field of the H_-BH_+ soliton found for the given intensity of the pump.

Let us mention that to reduce the time of the formation of the state, the pump is taken to be slightly inhomogeneous [shown in Fig. 9(a) by the blue line]. Otherwise, the soliton forms at a random point in the central part of the system and then slowly drifts towards the center. This motion happens because of the interaction of the soliton with the boundaries, which is very weak for long systems. This makes the soliton motion very slow and drastically increases the simulation time needed to observe the formation of a stationary state.

To observe the formation of moving solitons of $H_\pm BH_\pm$, it is more convenient to use an annular system with periodic boundary conditions. First, we need to grow a uniform hybrid state from initial weak noise. To do so, the uniform pump with intensity sufficient to set in the instability of the bright state is used. The development of the instability creates a stationary spatially uniform hybrid state with nonzero energy flow. The hybrid state forming at the pump $P = 0.2$ is the initial conditions for the protocol of the creation of the moving dissipative solitons. To obtain a nonuniform field distribution, we change the pump to the spatially nonuniform one shown in Fig. 10(b). In the area of low intensity, the pump cannot support the hybrid state and a stationary low-intensity bright state forms in this region. Thus, in the system appear the areas of the contact of the bright and the hybrid states.

It is possible to choose the difference of the minimum and the maximum pump intensities so that the hybrid states forming in the vicinity of the contact areas have the energy flow directed toward the bright state (to the area of the lower pump). This means that the interval filled with the bright state is between different hybrid states (one H_+ and another H_-).

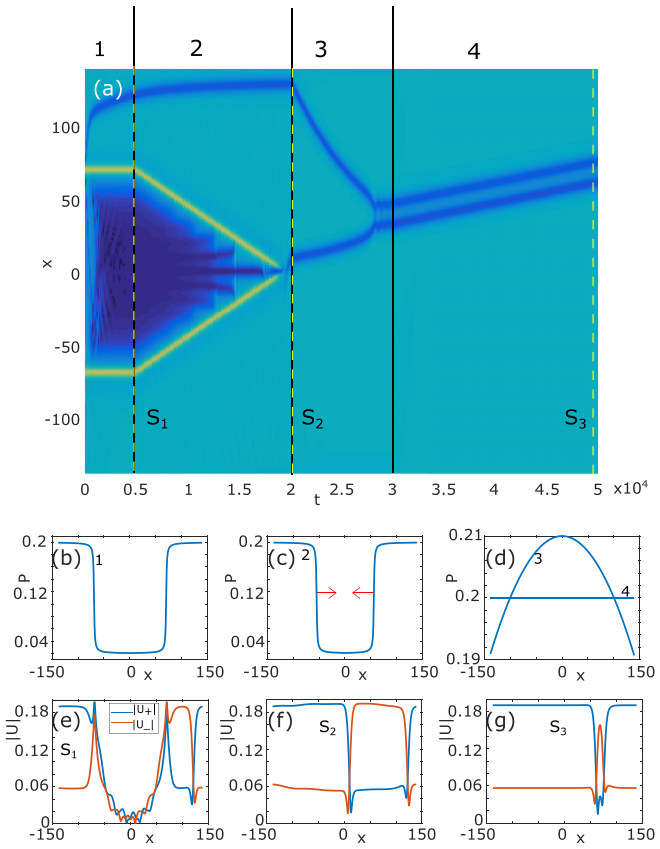

FIG. 10. Numerical simulation supporting the protocol of the formation of moving H_+BH_+ solitons suggested in the paper. (a) The temporal evolution of the intensity of the field. The intervals of different pumping regimes are marked by 1–4. The field distributions at the times marked by the vertical lines S_{1-3} are presented in panels (e)–(g) correspondingly. (b) The profile of the pump acting on the system within the interval 1 ($t < 5000$). (e) The quasistationary field formed by $t = 5000$. (c) The distribution of the pump amplitude within the time interval 2 ($5000 < t < 20\,000$). The area of the low intensity of the pump is slowly shrinking and, finally, the pump becomes spatially uniform. Schematically, the shrinking of the low pump area is indicated by the red arrows. (f) The field distributions at $t = 20\,000$. The pump distributions shown in (d) are for time intervals 3 ($20\,000 < t < 30\,000$) and 4 ($t > 30\,000$), and they are marked by the numbers 3 and 4 correspondingly. (g) The final distribution of the field ($t = 50\,000$). This field distribution perfectly coincides with the field distribution in the H_+BH_+ soliton existing at the pump $P = 0.21$.

But the system is annular and, thus, there must be an area where the H_+ and H_- states contact each other. This results in the formation of a dark dissipative soliton; see Fig. 10(a) where, in the region marked as 1 ($0 < t < 5000$), this dark soliton is clearly seen as well as two areas of contact of the bright and hybrid states. The distribution of the quasistationary fields as functions of the x coordinate is also shown in Fig. 10(e).

Then, at $t = 5000$, we start changing the pump, gradually reducing the width of the low-intensity pump; see Fig. 10(c). At $t = 20\,000$, the pump becomes spatially uniform and a new dark dissipative soliton H_+BH_- appears in the system. The region marked as 2 in Fig. 10(a) shows this process. So now there are two dark solitons in the system: one of them is the H_+BH_- soliton and the other is the H_-BH_+ soliton; see Fig. 10(f) showing the distribution of the fields.

A moving H_+BH_+ or H_-BH_- soliton can now be created by a gentle collision of the two dark solitons. To do so, we slightly change the shape of the pump, making it slightly nonuniform. The dark solitons H_+BH_- and H_-BH_+ move in opposite directions in the nonuniform pump: one soliton moves down and the other moves against the gradient of the pump intensity. This process is seen in the time interval $20\,000 < t < 30\,000$ marked as 3 in Fig. 10(a) for the pump shown in Fig. 10(d). After collisions of the solitons, a moving soliton H_+BH_+ appears; the fields distribution in this soliton is illustrated in Fig. 10(g). It is worth noting here that by changing the shape of the pump, it is possible to swap the sides of the colliding solitons and, thus, produce a H_-BH_- soliton.

At $t = 30\,000$, the pump is made uniform again and one can see that there is a stable dissipative soliton moving in the system [region 4 in Fig. 10(a)]. Thus, we can conclude that the suggested protocol allows one to create the dissipative solitons moving either clockwise or counterclockwise in the pumped annular system. Let us remark here that the suggested technique can also be used for the creation of more complex soliton structures.

So we can say that the protocols of possible experimental observation of the solitons are suggested and verified. This brings us to the end of this section and we proceed to the next one, where the main results of the work are summarized.

V. CONCLUSION

In this paper, we have considered the switching waves connecting the states with broken (hybrid states) and unbroken (bright states) symmetries. As discussed above, the states with broken symmetry have nonzero energy flow and, thus, the domain walls depend on the relative positions of the connected states (the domain wall connecting the BS on the left and the HS on the right is not equivalent to the domain wall connecting the HS on the left to the BS on the right). The domain walls are classified and their bifurcation diagrams are found and discussed.

It is shown that the domain walls can form a bound state that can be called dissipative solitons. An interesting finding is that the dissipative solitons can be moving and the direction of the motion is defined by the symmetries of the soliton background. The stability of the dissipative solitons is studied and it is shown that the solitons can be stable and so can be observed experimentally. In the paper, we also suggested and verified numerically the protocols allowing one to create the discussed solitons.

ACKNOWLEDGMENTS

The authors would like to express great appreciation to Professor N. N. Rosanov for fruitful discussions. The authors acknowledge the financial support provided by the Russian Fund for Basic Research (Grant "Aspiranty" No. 20-32-90227) and by the Ministry of Science and Higher Education of the Russian Federation (Megagrant No. 14.Y26.31.0015).

[1] N. N. Rozanov, Hysteresis phenomena in distributed optical systems, Zh. Eksp. Teor. Fiz. **80**, 96 (1981).

[2] D. W. McLaughlin, J. V. Moloney, and A. C. Newell, Solitary Waves as Fixed Points of Infinite-Dimensional Maps in an Optical Bistable Ring Cavity, Phys. Rev. Lett. **51**, 75 (1983).

[3] M. C. Cross and P. C. Hohenberg, Pattern formation outside of equilibrium, Rev. Mod. Phys. **65**, 851 (1993).

[4] B. A. Malomed, Optical domain walls, Phys. Rev. E **50**, 1565 (1994).

[5] K. Staliunas and V. J. Sánchez-Morcillo, Spatial-localized structures in degenerate optical parametric oscillators, Phys. Rev. A **57**, 1454 (1998).

[6] S. Coen, M. Tlidi, P. Emplit, and M. Haelterman, Convection Versus Dispersion in Optical Bistability, Phys. Rev. Lett. **83**, 2328 (1999).

[7] N. N. Rosanov and G. V. Khodova, Diffractive autosolitons in nonlinear interferometers, J. Opt. Soc. Am. B **7**, 1057 (1990).

[8] N. Rozanov, A. Fedorov, S. Fedorov, and G. Khodova, Particle-like light structures in a wide-aperture laser with saturable absorption, JETP **80**, 199 (1995).

[9] N. Rozanov, Dissipative optical solitons, J. Opt. Technol. **76**, 187 (2009).

[10] D. V. Skryabin, Instabilities of cavity solitons in optical parametric oscillators, Phys. Rev. E **60**, R3508 (1999).

[11] P. Coullet, C. Riera, and C. Tresser, Stable Static Localized Structures in One Dimension, Phys. Rev. Lett. **84**, 3069 (2000).

[12] U. Peschel, D. Michaelis, and C. O. Weiss, Spatial solitons in optical cavities, IEEE J. Quantum Electron. **39**, 51 (2003).

[13] D. Gomila and G.-L. Oppo, Subcritical patterns and dissipative solitons due to intracavity photonic crystals, Phys. Rev. A **76**, 043823 (2007).

[14] A. R. Champneys and A. V. Yulin, Discrete snaking: Multiple cavity solitons in saturable media, SIAM J. Appl. Dyn. Syst. **9**, 391 (2010).

[15] K. Kieu, W. H. Renninger, A. Chong, and F. W. Wise, Sub-100 fs pulses at watt-level powers from a dissipative-soliton fiber laser, Opt. Lett. **34**, 593 (2009).

[16] C. Lecaplain, B. Ortaç, and A. Hideur, High-energy femtosecond pulses from a dissipative soliton fiber laser, Opt. Lett. **34**, 3731 (2009).

[17] L. Carletti, S. S. Kruk, A. A. Bogdanov, C. De Angelis, and Y. Kivshar, High-harmonic generation at the nanoscale boosted by bound states in the continuum, Phys. Rev. Res. **1**, 023016 (2019).

[18] K. Koshelev, S. Kruk, E. Melik-Gaykazyan, J.-H. Choi, A. Bogdanov, H.-G. Park, and Y. Kivshar, Subwavelength dielectric resonators for nonlinear nanophotonics, Science **367**, 288 (2020).

[19] A. Kodigala, T. Lepetit, Q. Gu, B. Bahari, Y. Fainman, and B. Kanté, Lasing action from photonic bound states in continuum, Nature (London) **541**, 196 (2017).

[20] D. Dolinina and A. Yulin, Spontaneous symmetry breaking of nonlinear states in optical cavities with radiative losses, Opt. Lett. **45**, 3781 (2020).

[21] C. O. Weiss, H. R. Telle, K. Staliunas, and M. Brambilla, Restless optical vortex, Phys. Rev. A **47**, R1616 (1993).

[22] S. V. Fedorov, A. G. Vladimirov, G. V. Khodova, and N. N. Rosanov, Effect of frequency detunings and finite relaxation rates on laser localized structures, Phys. Rev. E **61**, 5814 (2000).

[23] A. J. Scroggie, J. M. McSloy, and W. J. Firth, Self-propelled cavity solitons in semiconductor microcavities, Phys. Rev. E **66**, 036607 (2002).

[24] A. G. Vladimirov, D. V. Skryabin, G. Kozyreff, P. Mandel, and M. Tlidi, Bragg localized structures in a passive cavity with transverse modulation of the refractive index and the pump, Opt. Express **14**, 1 (2006).

[25] N. Rozanov, Asymmetric moving localized structures in a wide-aperture nonlinear interferometer, Opt. Spectrosc. **102**, 255 (2007).

[26] N. Rozanov, A. Shatsev, and S. Fedorov, Moving and oscillating transversely one-dimensional laser solitons, Opt. Spectrosc. **102**, 456 (2007).

[27] D. Turaev, M. Radziunas, and A. G. Vladimirov, Chaotic soliton walk in periodically modulated media, Phys. Rev. E **77**, 065201(R) (2008).

[28] M. Tlidi, A. G. Vladimirov, D. Pieroux, and D. Turaev, Spontaneous Motion of Cavity Solitons Induced by a Delayed Feedback, Phys. Rev. Lett. **103**, 103904 (2009).

[29] O. A. Egorov and F. Lederer, Spontaneously walking discrete cavity solitons, Opt. Lett. **38**, 1010 (2013).

[30] C. Mejía-Cortés, R. A. Vicencio, and B. A. Malomed, Mobility of solitons in one-dimensional lattices with the cubic-quintic nonlinearity, Phys. Rev. E **88**, 052901 (2013).

[31] A. J. Alvarez-Socorro, M. G. Clerc, and M. Tlidi, Spontaneous motion of localized structures induced by parity symmetry breaking transition, Chaos: Interdiscip. J. Nonlinear Sci. **28**, 053119 (2018).

[32] P. Coullet, J. Lega, B. Houchmandzadeh, and J. Lajzerowicz, Breaking Chirality in Nonequilibrium Systems, Phys. Rev. Lett. **65**, 1352 (1990).

[33] D. Michaelis, U. Peschel, F. Lederer, D. V. Skryabin, and W. J. Firth, Universal criterion and amplitude equation for a nonequilibrium Ising-Bloch transition, Phys. Rev. E **63**, 066602 (2001).

[34] K. Staliunas and V. J. Sánchez-Morcillo, Ising-Bloch transition for spatially extended patterns, Phys. Rev. E **72**, 016203 (2005).

[35] D. Gomila, P. Colet, and D. Walgraef, Theory for the Spatiotemporal Dynamics of Domain Walls Close to a Nonequilibrium Ising-Bloch Transition, Phys. Rev. Lett. **114**, 084101 (2015).

[36] M. G. Clerc, S. Coulibaly, and M. Tlidi, Time-delayed nonlocal response inducing traveling temporal localized structures, Phys. Rev. Res. **2**, 013024 (2020).

[37] M. G. Clerc, S. Coulibaly, P. Parra-Rivas, and M. Tlidi, Nonlocal raman response in Kerr resonators: Moving temporal localized structures and bifurcation structure, Chaos: Interdiscip. J. Nonlinear Sci. **30**, 083111 (2020).

[38] P. Parra-Rivas, S. Coulibaly, M. G. Clerc, and M. Tlidi, Influence of stimulated Raman scattering on Kerr domain walls and localized structures, Phys. Rev. A **103**, 013507 (2021).

[39] S. D. Krasikov, A. A. Bogdanov, and I. V. Iorsh, Nonlinear bound states in the continuum of a one-dimensional photonic crystal slab, Phys. Rev. B **97**, 224309 (2018).

[40] G. P. Agrawal, *Nonlinear Fiber Optics* (Elsevier Science, Amsterdam, 2013).

[41] T. X. Tran and N. N. Rosanov, Conservative and dissipative fiber Bragg solitons (A review), Opt. Spectrosc. **105**, 393 (2008).

[42] A. V. Yulin, A. Aladyshkina, and A. S. Shalin, Motion of dissipative optical fronts under the action of an oscillating pump, Phys. Rev. E **94**, 022205 (2016).

[43] G. Kozyreff and S. J. Chapman, Asymptotics of Large Bound States of Localized Structures, Phys. Rev. Lett. **97**, 044502 (2006).

[44] J. Burke and E. Knobloch, Homoclinic snaking: Structure and stability, Chaos: Interdiscip. J. Nonlin. Sci. **17**, 037102 (2007).

[45] M. Tlidi and L. Gelens, High-order dispersion stabilizes dark dissipative solitons in all-fiber cavities, Opt. Lett. **35**, 306 (2010).

[46] V. B. Taranenko, C. O. Weiss, and W. Stolz, Spatial solitons in a pumped semiconductor resonator, Opt. Lett. **26**, 1574 (2001).

[47] P. M. Walker, L. Tinkler, D. V. Skryabin, A. Yulin, B. Royall, I. Farrer, D. A. Ritchie, M. S. Skolnick, and D. N. Krizhanovskii, Ultra-low-power hybrid light–matter solitons, Nat. Commun. **6**, 8317 (2015).